International Journal of Microwave and Wireless Technologies

cambridge.org/mrf

Tunable attenuating diplexer using miniaturized multilayer graphene pads

Sai Haranadh Akkapanthula and Srujana Kagita

Department of Electrical Engineering, Indian Institute of Technology Tirupati, Yerpedu, India

Research Paper

Cite this article: Akkapanthula SH, Kagita S (2024) Tunable attenuating diplexer using miniaturized multilayer graphene pads. *International Journal of Microwave and Wireless Technologies* **16**(10), 1722–1729. https://doi.org/10.1017/S1759078725000066

Received: 11 June 2024
Revised: 2 January 2025
Accepted: 9 January 2025

Keywords:
coupled line filter; diplexer; multilayer graphene; tunable attenuator; voltage bias

Corresponding author:
Sai Haranadh Akkapanthula;
Email: ee22d001@iittp.ac.in

Abstract

In this article, a coupled line diplexer (operating at 2.4 GHz and 3.5 GHz) which can be used as single-band filter with tunable attenuation characteristics in the pass band has been designed. Multilayer graphene (MLG) pads are used to achieve tunable features in this circuit. The graphene pads are placed at each branch of the diplexer. Single-band tunable attenuation characteristics are achieved by applying bias to graphene pads placed at optimum locations on the filter. The proposed tunable coupled line attenuating diplexer is realized on FR-4 glass epoxy substrate of thickness 1.58 mm with a total size of 45×75 mm^2. By varying the bias voltage (0 V –6 V) of MLG pads the resistance of graphene pad placed in the circuit gets decreases thereby attenuating/controlling the transmission power to the other port in the required band. In lower pass band (2.28–2.55 GHz) the signal is attenuated from 3 to 10.8 dB and in higher pass band (3.2–3.58 GHz) signal is attenuated from 5 to 13 dB. Simulations of the structure with and without graphene pads have been carried out and are in good agreement with measured results.

Introduction

One of the most essential components of Radio Frequency (RF) front end systems is a diplexer which routes signals of different frequencies through separate branches of the circuit. Earlier, diplexers are made using waveguide technology for high power handling. Later, microstrip technology enabled planar integration of these components. Various topologies like coupled line diplexer [1], stepped impedance resonator-based diplexer [2], Coplanar Wave Guide (CPW) based diplexer with semi lumped elements [3] have been discussed in literature. The crucial part in designing a diplexer is input matching [4]. Some planar diplexers have been discussed in references [5–9]. This matching is done in such a way that both the frequencies do not interfere with each other in respective bands. In this paper, coupled line filter-based diplexer is designed to incorporate tunability feature using graphene pads.

Investigation on graphene-based microwave devices is being carried out by researchers from past few years. In the initial days researchers found its importance in Terahertz frequency range, later researchers are trying to push the limits of graphene to check its potential in microwave band. Graphene is a material having a unique property. Its fermi level is of cone shape [10] and requires very small energy to transform from valance band to conduction band. During this transition, conductivity of material varies. This feature has potential applications in microwave region as well. Exploring the characteristics of graphene in microwave range began by making attenuator circuits using tiny graphene pads. Various circuits such as microstrip attenuators [11–15], CPW based attenuators [16, 17], Substrate Integrated Wave Guide (SIW) based attenuators [18], half-mode SIW attenuators [19] have been discussed in literature. In reference [20], tunable filtering attenuator was made by integration of graphene. Similarly tunable attenuators with spoof surface plasmon polaritons using graphene have been tested on flexible circuits in references [21, 22]. Power dividers [23, 24] and antennas [25–28] with tunable attenuation characteristics are also reported. The usage of graphene in microwave range was extended to design absorbers [29, 30]. The characterization of graphene is discussed in references [31–33].

In this paper, the features of graphene material are used to suppress the signals coming out of either of the two channels of the diplexer. Due to this, the designer can continuously regulate the power obtained at two channels of the diplexer. The design is implemented in two bands with frequencies centered at 2.4 and 3.5 GHz.

Design of coupled line diplexer

Figure 1 shows the parallel coupled line diplexer comprising of two second-order filters connected to 50 Ω line. The top section (Branch 1) in the diplexer is designed to operate at 2.4 GHz and having a pass band ranging from 2.28 to 2.55 GHz. The bottom section (Branch 2) is designed at a center frequency of 3.5 GHz having a pass band from 3.2 to 3.58 GHz.

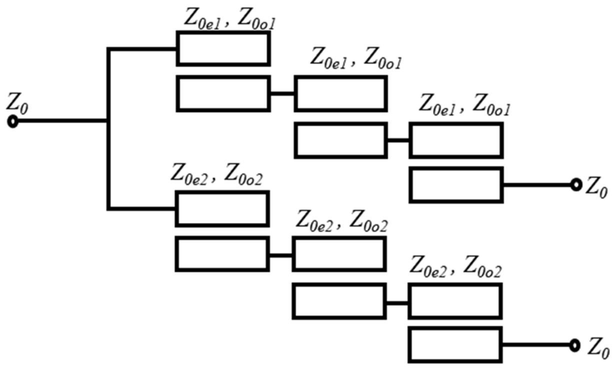

Figure 1. Schematic of coupled line diplexer.

The even- and odd-mode capacitances of the individual filters have been calculated using equations (1[a] & 1[b]) respectively. Appropriate matching at the input reduces the interference between the two pass bands. This input matching can be done by using different lengths of a 50 Ω transmission line. The input line connecting to branch 1, which is operating at lower band should provide high impedance for band 2, thereby obstructing the passage of the signal and vice versa.

$$Z_{0e} = Z_0\left[1 + JZ_0 + (JZ_0)^2\right] \quad 1(a)$$

$$Z_{0o} = Z_0\left[1 - JZ_0 + (JZ_0)^2\right] \quad 1(b)$$

where, admittance inverter constants can be found using equations 2(a)–(c).

$$Z_0J_1 = \sqrt{\frac{\pi\Delta}{2g_1}} \quad 2(a)$$

$$Z_0J_n = \frac{\pi\Delta}{2\sqrt{g_{n-1}g_n}} \quad 2(b)$$

$$Z_0J_{N+1} = \sqrt{\frac{\pi\Delta}{2g_Ng_{N+1}}} \quad 2(c)$$

The schematic of the diplexer circuit in Fig. 1 is simulated in advance design systems. Figure 2(a) and (b) shows S_{11} curves in smith chart validating matching of the circuit at the input of branches 1 and 2, respectively.

The relation between the spacing "S" and height of substrate "h" is given [34] as

$$0.05 \leqslant \frac{s}{h} \leqslant 2 for \in_r \geqslant 1 \quad (3)$$

The lengths ($W1$, $W2$, $W3$, and $W4$) of coupled microstrip resonators are considered approximately as $\frac{\lambda_g}{2}$ for bandpass regions of each filter section.

Theoretical calculation of coupled line section even- and odd-mode impedances for a given microstrip line configuration

Z_{0o} and Z_{0e} of second order coupled line filters are calculated using equations 4(a)–(a_1) [34, 35] and are given in Table 1(a) and (b). The equivalent widths and lengths of microstrip lines calculated for this design are also given in Table 2.

For a coupled microstrip line of width W, spacing "s" and height "h" fabricated on a substrate having $\varepsilon_r = 4.4$, the following equations apply. For the case where,

$$0.1 \leqslant u\left(=\frac{W}{h}\right) \leqslant 10, 0.1 \leqslant g\left(=\frac{s}{h}\right) \leqslant 10, 1 \leqslant \varepsilon_r \leqslant 18$$

$Z_{0_{\text{odd}}}$ and $Z_{0_{\text{even}}}$ are calculated by following equations

$$Z_{0_{\text{odd}}} = Z_{0_{\text{surf}}} \cdot \left[\frac{\sqrt{\frac{\varepsilon_{r_{\text{eff}}}}{\varepsilon_{r_{\text{eff},o}}}}}{1 - \left(\frac{Z_{0_{\text{surf}}}}{\eta_0} \cdot q_{10} \cdot \sqrt{\varepsilon_{r_{\text{eff}}}}\right)}\right] \quad 4(a)$$

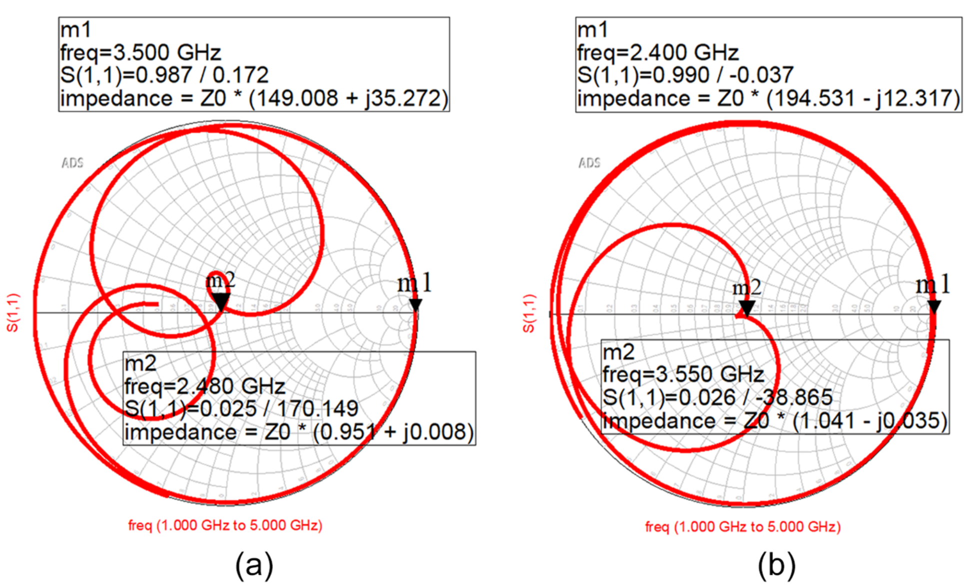

Figure 2. Smith chart showing matching of diplexer for branch 1 & branch 2. 2(a) Branch 1 - high impedance for higher band & 2(b) branch 2 - high impedance for lower band.

https://doi.org/10.1017/S1759078725000066 Published online by Cambridge University Press

Table 1. (a) Even- and odd-mode impedances of section 1. (b) Even- and odd-mode impedances of section 2

Z_{0e} (Ω)	Z_{0o} (Ω)	Spacing (mm)	Width (mm)
68.4	31.6	0.26	2.612
50.53	36.98	1.1	3.664
68.4	31.6	0.26	2.612
For section 2,			
65.99	34	0.355	2.713
50.29	40.06	1.688	3.53
65.99	34	0.355	2.713

Table 2. Optimized dimensions of T-CLAD using MLG in mm

L	W	L_1	W_1	W_2	W_3	Lm_2	Lm_4
45	75	3	17	11.7	16.8	3.71	3.55
W_4	S_1	S_2	S_3	S_4	Lm_1	Lm_3	
11.3	0.15	0.38	0.65	1.2	2.645	2.765	

$$Z_{0_{\text{even}}} = Z_{0_{\text{surf}}} \cdot \left[\frac{\sqrt{\frac{\varepsilon_{r_{\text{eff}}}}{\varepsilon_{r_{\text{eff},e}}}}}{1 - \frac{Z_{0_{\text{surf}}}}{\eta_0} . q_4 \cdot \sqrt{\varepsilon_{r_{\text{eff}}}}} \right] \quad 4(b)$$

Where $Z_{0_{\text{odd}}}, Z_{0_{\text{even}}}$ are the odd- and even-mode impedances of the coupled microstrip lines. And $Z_{0_{\text{surf}}}$ is surface impedance, $\varepsilon_{r_{\text{eff}}}$ is the effective dielectric constant, η_0 .is free space impedance, $\varepsilon_{r_{\text{eff},o}}$ .is static odd-mode effective dielectric constant, $\varepsilon_{r_{\text{eff},e}}$ is static even-mode effective dielectric constant. The variables q_4 and q_{10} are constants given by equations 4(n) and 4(o).

For $\frac{W}{h} \leqslant 1$ the effective dielectric constant is calculated as

$$\varepsilon_{r_{\text{eff}}} = \frac{\varepsilon_r + 1}{2} + \frac{\varepsilon_r - 1}{2} . \left(\sqrt{\frac{W}{W + 12h}} + 0.04 \left(1 - \frac{W}{h}\right)^2 \right) \quad 4(c)$$

When $\frac{W}{h} \geqslant 1$ the effective dielectric constant is calculated as

$$\varepsilon_{r_{\text{eff}}} = \frac{\varepsilon_r + 1}{2} + \frac{\varepsilon_r - 1}{2} . \left(\sqrt{\frac{W}{W + 12h}} \right) \quad 4(d)$$

In our design $\frac{W}{h} \geqslant 1$.

To calculate surface impedance $Z_{0_{\text{surf}}}$ we use the following equations from 4(e) to 4(g)

$$Z_{0_{\text{surf}}} = \frac{\eta_0}{2\pi\sqrt{2}\sqrt{\varepsilon_{r_{\text{eff}}} + 1}} . \ln \left(1 + \left(4 . \frac{h}{W_{\text{eff}}} \right) . \left(\left(4 . \frac{h}{W_{\text{eff}}} \right) . \frac{14 . \varepsilon_{r_{\text{eff}}} + 8}{11 . \varepsilon_{r_{\text{eff}}}} \right) + temp \right) \quad 4(e)$$

Where W_{eff} is effective width of the line

$$W_{\text{eff}} = W + \frac{t}{\pi} . \ln \left(\frac{4e}{\sqrt{\left(\frac{t}{h}\right)^2 + \left(\frac{t}{W\pi + 1.1\pi}\right)^2}} \right) . \frac{\varepsilon_{r_{\text{eff}}} + 1}{2 . \varepsilon_{r_{\text{eff}}}} \quad 4(f)$$

Where ′temp′ is a constant and given by,

$$temp = \sqrt{16 \left(\frac{h}{W_{\text{eff}}}\right)^2 . \left(\frac{14 . \in_{r_{\text{eff}}} + 8}{11 . \in_{r_{\text{eff}}}}\right)^2 + \left(\frac{\in_{r_{\text{eff}}} + 1}{2 . \in_{r_{\text{eff}}}}\right) . \pi^2} \quad 4(g)$$

To evaluate $\varepsilon_{r_{\text{eff},o}}$ and $\varepsilon_{r_{\text{eff},e}}$ we use equations 4(h) to 4(q)

$$\varepsilon_{r_{\text{eff},o}} = \left(0.5\left(\varepsilon_r + 1\right) + a_0 - \varepsilon_{r_{\text{eff}}} . e^{-c_0 \cdot g^{d_0}}\right) + \varepsilon_{r_{\text{eff}}} \quad 4(h)$$

$$a_0 = 0.7287 \left(\varepsilon_{r_{\text{eff}}} - \frac{\varepsilon_r + 1}{2}\right) . \left(\sqrt{1 - e^{-0.179u}}\right) \quad 4(i)$$

$$b_0 = \frac{0.747 . \varepsilon_r}{0.15 + \varepsilon_r} \quad 4(j)$$

$$c_0 = b_0 - \left(b_0 - 0.207\right) . e^{-0.414u} \quad 4(k)$$

$$d_0 = 0.593 + 0.694 e^{-0.562u} \quad 4(l)$$

$$g = \frac{s}{h} \quad 4(m)$$

$$\varepsilon_{r_{\text{eff},e}} = \frac{\varepsilon_r + 1}{2} + \frac{\varepsilon_r - 1}{2} . \left(1 + \frac{10}{v}\right)^{-ae(v) . b_e(\varepsilon_r)} \quad 4(n)$$

Where,

$$v = \frac{u . \left(20 + g^2\right)}{10 + g^2} + g e^{-g} \quad 4(o)$$

$$ae\left(v\right) = 1 + \frac{\ln\left(\frac{v^4 + \left(\frac{v}{52}\right)^2}{v^4 + 0.432}\right)}{49} + \frac{\ln\left(1 + \left(\frac{v}{18.1}\right)^3\right)}{18.7} \quad 4(p)$$

$$b_e\left(\varepsilon_r\right) = 0.564 \left(\frac{\varepsilon_r - 0.9}{\varepsilon_r + 3}\right)^{0.053} \quad 4(q)$$

To evaluate constants q_4, q_{10} given in equation 4(a) & 4(b) the following equations are used

$$q_4 = \frac{2 * q_1}{q_2 * \left(e^{-g} * u^{-q_3} + \left(2 - e^{-g}\right) * u^{-q_3}\right)} \quad 4(r)$$

$$q_{10} = \left(\frac{1}{q2}\right) * \left(q_2 * q_4 - q_5 * e^{(\ln(u) * q_6 * u^{-q_9})}\right) \quad 4(s)$$

The constants q_1, q_9 required to evaluate q_4 and q_{10} are given by

$$q_1 = 0.8695 * \ u^{0.194} \quad 4(t)$$

$$q_2 = 1 + 0.7519 * g + 1.89 * g^{2.31} \quad 4(u)$$

$$q_3 = 0.1975 + \left(16.6 + \left(\frac{8.4}{g}\right)^6\right)^{-0.387} + \frac{1}{241} \ln \left(\frac{g^{10}}{1 + \left(\frac{g}{3.4}\right)^{10}}\right) \quad 4(v)$$

$$q_5 = 1.794 + 1.14 * \ln \left(1 + \left(\frac{0.638}{g + 0.517 * g^{2.43}}\right)\right) \quad 4(w)$$

https://doi.org/10.1017/S1759078725000066 Published online by Cambridge University Press

$$q_6 = 0.2305 + \frac{1}{281.3} * \ln\left(\frac{g^{10}}{1+\left(\frac{g}{5.8}\right)^{10}}\right) + \frac{1}{5.1} * \ln(1+0.598) * g^{1.154} \quad 4(x)$$

$$q_7 = \frac{10+190 * g^2}{1+82.3 * g^3} \quad 4(y)$$

$$q_8 = e^{\left(-6.5-0.95*\ln(g)-\left(\frac{g}{0.15}\right)^2\right)} \quad 4(z)$$

$$q_9 = \ln(q_7) * \left(q_8 + \frac{1}{16.5}\right) \quad 4(a_1)$$

In this design, considering the thickness of the line as $t = 0.035$ mm, the height of substrate $h = 1.58$ mm, $\varepsilon_r = 4.4$, the following values are obtained for odd- and even-mode impedances are obtained for coupled line sections 1 & 2 designed for f_1 and f_2 frequencies for a given spacing "s" and width W of the lines.

Based on the impedances obtained, using microstrip line theory [34] the width of the lines have been calculated. The design parameters have been optimized for better results and the optimized dimensions of the circuit are given in the following table.

Implementation of the design in 3D EM software

The proposed tunable coupled line attenuating diplexer (T-CLAD) structure simulated in 3D Electro Magnetic (EM) solver Ansys HFSS is shown in Fig. 3(a). After optimization, the design is realized on FR-4 substrate of thickness 1.58 mm and having electrical properties $\varepsilon_r = 4.4$ and $\tan\delta = 0.025$. Dimensions of the circuit labelled in Fig. 3(a) are given in Table 1. The measurements are carried out using Keysight network analyzer PNA N5224B. Simulated and measured results of circuit without graphene pads are plotted in Fig. 3(b). Later Graphene pads are placed at locations shown in Fig. 3(a). As Graphene is lossy material with high dielectric constant and high loss tangent [31–33], it is effecting the transmission parameters slightly. Due to the standard losses of dielectric, there exist some transmission losses initially in both pass bands.

Characterization of MLG pads

Preparation and testing of MLG pads.

Commercially available high-purity multilayer graphene (MLG) of flake size 1–5 μm has been chosen for making graphene pads. Initially, this MLG is mixed with isopropyl alcohol (IPA) at 10 mg/ml. This mixture is sonicated for 20 minutes to get the graphene particles dispersed uniformly in the liquid. Now this dispersed graphene liquid is transferred to the desired position on the circuit carefully using a dropper as shown in Fig. 4(a). The IPA in the mixture gets evaporated after some time leaving the pure graphene as a resistive sheet. The resistance of the graphene pad depends on the thickness and area of the pad. Controlled dropping of graphene liquid is required based on the requirement. Applying bias to these pads varies the resistance. Figure 4(b) shows the plot of current vs applied voltage and resistance vs applied voltage of the pads placed in the circuit. Further increase in bias voltage (>6 V) leads to the breakdown of graphene pads.

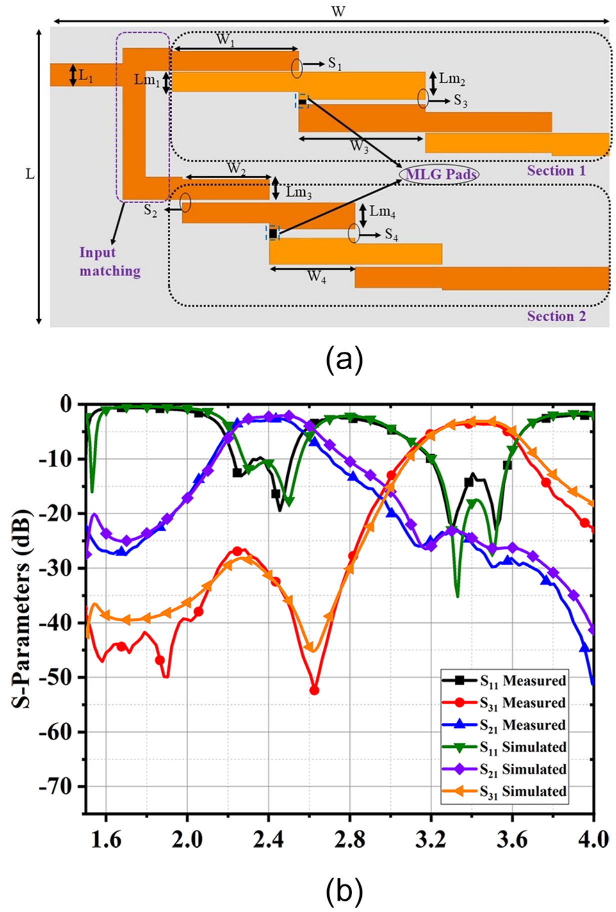

Figure 3. Proposed tunable attenuating diplexer using MLG pads. (a) Schematic with graphene pads & (b) simulated and measured S-parameters of proposed diplexer without graphene.

Results & discussion

The MLG pads are placed at the edges of the center coupled-line section of the design for both branches as shown in Fig. 5(a) (circled). Initial resistance of graphene pads is around 250 Ω. As graphene is a resistive sheet, the coupling between the sections is slightly disturbed and the insertion loss in the higher band has slightly increased. Bias is applied to each of these pads and the resistance of pads is varied in branch 1 and branch 2 separately. The fabricated prototype of proposed T-CLAD and corresponding Measured and simulated S-parameters of the circuit after placing the graphene pads are shown in Fig. 5(a) and (b), respectively.

The size of graphene pads placed for branch 1 is 0.65 × 1 mm and for branch 2 it is 1.2 × 1 mm. A variable three-channel DC multiple power supply (Model Number: PSD3304) from Scientific company is used to apply DC bias to the graphene pads as shown in Fig. 6 (a). As the coupler sections inherently block DC, there is no need for a bias tee for additional protection while carrying out this experiment. When the graphene pad in branch 1 is

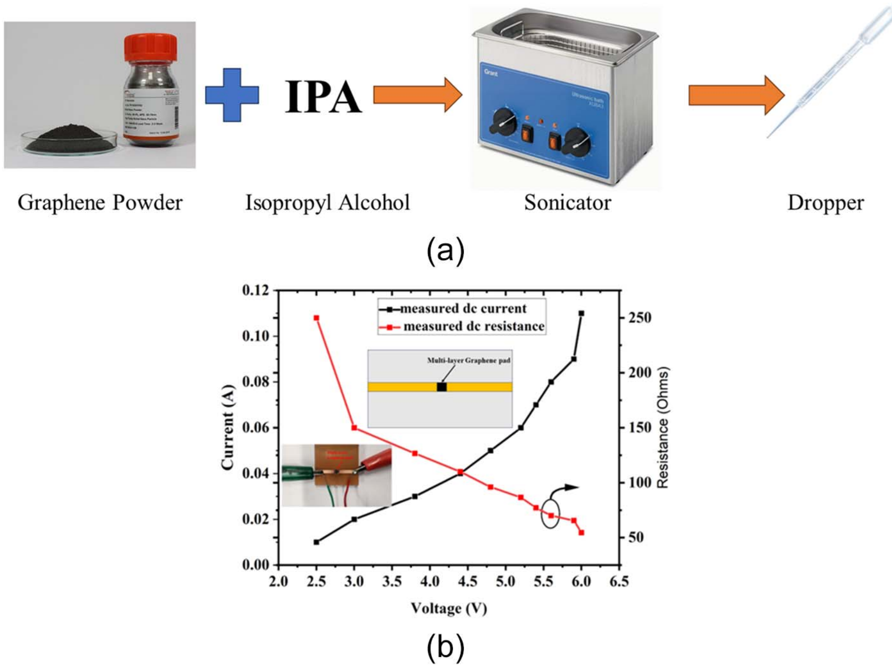

Figure 4. (a) Preparation of Graphene pads & (b) Measured resistance of MLG pad and voltage vs current plot.

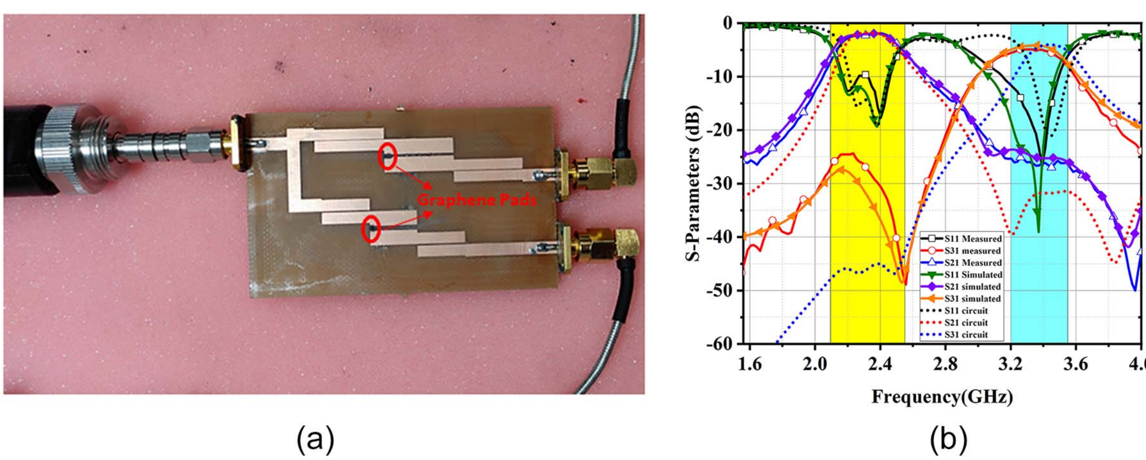

Figure 5. Proposed T-CLAD and its S-parameters. (a) Fabricated prototype of T-CLAD with MLG pads & (b) S-parameters without biasing the graphene.

biased with voltage varying from 0 to 6 V, there is a corresponding change in resistance of the graphene pad from 250 to 54 Ω. Due to this attenuation in branch 1 is varied from 4.6 to 10.3 dB. Figure 6(b) shows the simulated and measured S-parameters corresponding to the biasing of the graphene pad in branch 1. The graphene pad in branch 2 is also biased similarly, resulting in variable attenuation from 4.8 to 14.1 dB in the second operating band. Measured and simulated results obtained by biasing graphene pad in branch 2 are shown in Fig. 6(c). Figure 6(a) shows the test setup of the circuit and biasing of graphene pads in the fabricated circuit.

This circuit can be used to control the power levels of signals appearing at the two branches of the diplexer. By biasing the graphene pads in branch 1 and 2, the power levels of the two operating bands can be controlled simultaneously. This circuit has applications in reconfigurable Bluetooth, WLAN systems. This concept can be applied to any other desired bands of interest. Multiple graphene pads can also be placed to obtain additional attenuation. However, insertion loss of circuit might degrade by using more graphene pads. Table 3 gives the comparison of proposed attenuating diplexer with existing literature.

In references [5, 6] tunable diplexers are realized using varactor diodes. In reference [5], a total of nearly 18 varactor diodes are used to obtain the desired tuning characteristics making the circuit very complex and power-hungry. In reference [6], a total of 10 varactor diodes are used achieve the desired characteristics. In both these circuits, the use of several diodes makes these circuits very cumbersome. In this paper, by using two very tiny graphene pads we are able to achieve considerable attenuation levels in the pass band with tolerable insertion loss using extremely low powers (around 6 mW). In reference [9] the size of the two graphene pads is almost 10 times larger than the pads used in our design. The use of such large pads will result in larger surface resistance leading to higher insertion losses. This work has the advantage of using a very simple diplexer design and a relatively easier

https://doi.org/10.1017/S1759078725000066 Published online by Cambridge University Press

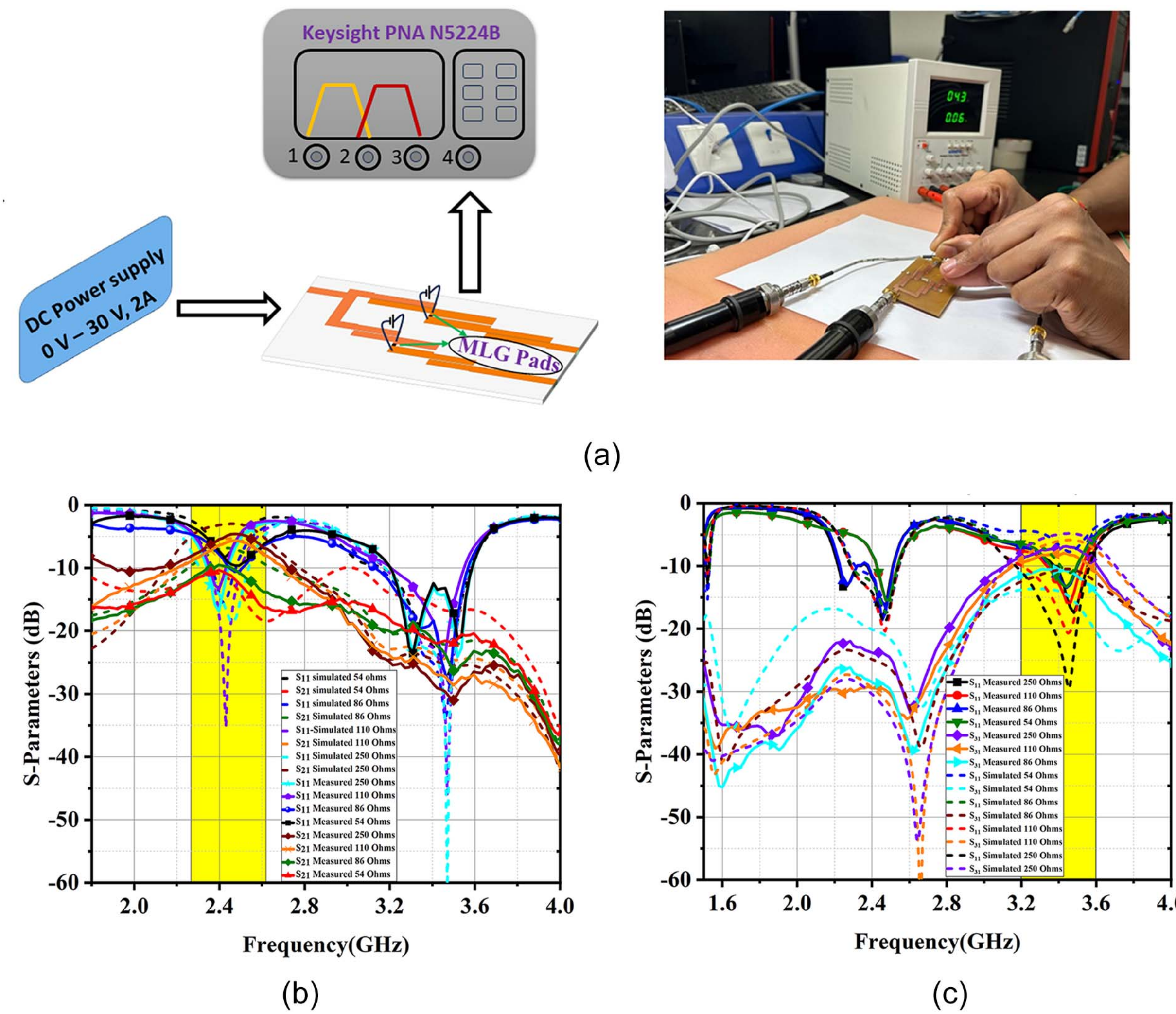

Figure 6. (a) Test setup of T-CLAD with graphene pads, (b) variation in lower pass band, & (c) variation in higher pass band.

Table 3. Comparison of proposed attenuating diplexer with existing literature

Ref	Frequency bands (GHz)	Measured IL (dB)	Tuning method	No. of graphene pads	Size of graphene pad	Attenuation in the bands(dB)
[5]	0.5–2	4.3/7.7	Varactor diode tuned	–	–	4.35–2.5 7.72–3.6
[6]	1.1/1.62	6.8/7.1	Varactor diode tuned	–	–	6.8–3/2.6–7.1
[9]	1.4/2.4	4	Graphene pad	2	5.15 mm × 10 mm	7
This work	***2.4/3.5***	***4***	***Graphene pad***	***2***	***0.65 mm × 1 mm 1.2 mm × 1 mm***	***5.7 (band 1) 9 (band 2)***

bias mechanism which consumes very low power for its tunable operation.

Conclusion

A diplexer circuit with tunable attenuation characteristics using MLG pads has been proposed and fabricated. Tiny graphene pads are placed in between the coupled sections of each filter and biased from 0 to 6 V correspondingly observed a change in resistance of graphene pad (from 250 to 54 Ω) is observed. This change in resistance results in reducing the power levels of transmission signal in two operating bands individually. This concept can be further extended to multiplexer (more than two operating bands) circuits for wireless applications.

Competing interests. The authors have no conflict of interest.

References

1. **Idrees M, Khalid S, AbdulRehman M, Mushtaq B, Najam AI and Alhaisoni M** (2023) Design of a stub-loaded coupled line diplexer for IoT-based applications. In *IEEE Embedded Systems Letters*
2. **Puttadilok D, Eungdamrong D and Amornsaensak S** (2008) A microstrip diplexer filter using stepped-impedance resonators. In *2008 SICE Annual Conference*, Chofu, Japan, 59–62.
3. **Barth S and Iyer AK** (2020) Design of a broadband embedded CPW-mode diplexer using multiconductor transmission-line metamaterial techniques. 2020 IEEE International Symposium on Antennas and Propagation and North American Radio Science Meeting, Montreal, QC, Canada, 913–914
4. **Duan S, Li S and Xia Y** (2021) Microstrip line-based ultra-wideband diplexer design. 2021 IEEE International Workshop on Electromagnetics: Applications and Student Innovation Competition (iWEM), Guangzhou, China, 1–3.
5. **Xu J and Zhu Y** (2017) Tunable bandpass filter using a switched tunable diplexer technique. *IEEE Transactions on Industrial Electronics* **64**(4), 3118–3126.
6. **Xu J** (2016) A tunable diplexer based on mixed coupling varactor-tuned stepped-impedance resonators. *Microwave and Optical Technology Letters* **58**(6), 1469–1473.
7. **Rezaei A and Noori L** (2018) Novel compact microstrip diplexer for GSM applications. *International Journal of Microwave and Wireless Technologies* **10**(3), 313–317.
8. **Kumar A and Upadhyay DK** (2019) A compact planar diplexer based on via-free CRLH TL for WiMAX and WLAN applications. *International Journal of Microwave and Wireless Technologies* **11**(2), 130–138.
9. **Chen J, Zhu S, Liang L and Fan C** (2022) Microstrip bandpass diplexer with linear-tunable attenuation based on graphene flakes. *Materials Letters* **316**, 132059.
10. **Ghivela GC and Senguptac J** (2020) The promise of graphene: A survey of microwave devices based on graphene. *IEEE Microwave Magazine* **21**(2), 48–65.
11. **D'Agati N and Zec J** (2021) Laser-scribed graphene (LSG) fabrication method for microwave circuit applications. *IEEE Microwave and Wireless Components Letters* **31**(11), 1215–1218.
12. **Pierantoni L, Bozzi M, Moro R, Mencarelli D and Bellucci S** (2014) On the use of electrostatically doped graphene: Analysis of microwave attenuators. In *2014 International Conference on Numerical Electromagnetic Modeling and Optimization for RF, Microwave, and Terahertz Applications (NEMO)*, Pavia, Italy, 1–4.
13. **Pierantoni L, Mencarelli D, Bozzi M, Moro R and Bellucci S** (2014) Graphene-based electronically tunable microstrip attenuator. 2014 IEEE MTT-S International Microwave Symposium (IMS2014), Tampa, FL, USA, 1–3.
14. **Yasir M, Bistarelli S, Cataldo A, Bozzi M, Perregrini L and Bellucci S** (2017) Enhanced tunable microstrip attenuator based on few layer graphene flakes. *IEEE Microwave and Wireless Components Letters* **27**(4), 332–334.
15. **Zhang A-Q, Liu Z-G, Lu W-B and Chen H** (2019) Dynamically tunable attenuator on a graphene-based microstrip line. *IEEE Transactions on Microwave Theory & Techniques* **67**(2), 746–753.
16. **Wu B, Zhang Y, Zu H, Fan C and Lu W** (2019) Tunable grounded coplanar waveguide attenuator based on graphene nanoplates. *IEEE Microwave and Wireless Components Letters* **29**(5), 330–332.
17. **Zhang A-Q, Liu Z-G, Wei-Bing L and Chen H** (2019) Graphene-based dynamically tunable attenuator on a coplanar waveguide or a slotline. *IEEE Transactions on Microwave Theory & Techniques* **67**(1), 70–77.
18. **Zhang A-Q, Lu W-B, Liu Z-G, Chen H and Huang B-H** (2018) Dynamically tunable substrate-integrated-waveguide attenuator using graphene. *IEEE Transactions on Microwave Theory & Techniques* **66**(6), 3081–3089.
19. **Zhang A, Liu Z, Weibing L and Chen H** (2018) Graphene-based dynamically tunable attenuator on a half-mode substrate integrated waveguide. *Applied Physics Letters* **112**(16).
20. **Wu B, Fan C, Feng X, Zhao YT, Ning J, Wang D and Su T**(2020) Dynamically tunable filtering attenuator based on graphene integrated microstrip resonators. *IEEE Transactions on Microwave Theory & Techniques* **68**(12), 5270–5278.
21. **Zhang A-Q, Lu W-B, Liu Z-G, Wu B and Chen H** (2019) Flexible and dynamically tunable attenuator based on spoof surface plasmon polaritons waveguide loaded with graphene. *IEEE Transactions on Antennas and Propagation* **67**(8), 5582–5589.
22. **Chen Z-P, Lu W-B, Liu Z-G, Zhang A-Q, Wu B and Chen H** (2020) Dynamically tunable integrated device for attenuation, amplification, and transmission of SSPP using graphene. *IEEE Transactions on Antennas and Propagation* **68**(5), 3953–3962.
23. **Bian W, Hao-Ran Z, Xue B-Y, Zhao Y-T and Cheng QS** (2019) Flexible wideband power divider with high isolation incorporating spoof surface plasmon polaritons transition with graphene flake. *Applied Physics Express* **12**(2), 022008.
24. **Wu B, Zhang Y, Zhao Y, Zhang W and He L** (2018) Compact nine-way power divider with omnidirectional resistor based on graphene flake. *IEEE Microwave and Wireless Components Letters* **28**(9), 762–764.
25. **Tamagnone M, Gómez-Díaz JS, Mosig JR and Perruisseau-Carrier J** (2012) Analysis and design of terahertz antennas based on plasmonic resonant graphene sheets. *Journal of Applied Physics* **112**(11).
26. **Zu R, Wu B, Zhang Y-H, Zhao Y-T, Song R-G and He D-P** (2020) Circularly polarized wearable antenna with low profile and low specific absorption rate using highly conductive graphene film. *IEEE Antennas and Wireless Propagation Letters* **19**(12), 2354–2358.
27. **Fan C, Wu B, Hu Y, Zhao Y and Su T** (June 2020) Millimeter-wave pattern reconfigurable vivaldi antenna using tunable resistor based on graphene. *IEEE Transactions on Antennas and Propagation* **68**(6), 4939–4943.
28. **Wang J, Lu W-B, Liu Z-G, Zhang A-Q and Chen H** (2020) Graphene-based microwave antennas with reconfigurable pattern. *IEEE Transactions on Antennas and Propagation* **68**(4), 2504–2510.
29. **Zhang J, Zhenfei L, Shao L and Zhu W** (2021) Dynamical absorption manipulation in a graphene-based optically transparent and flexible metasurface. *Carbon* **176**, 374–382.
30. **Huang C, Zhao B, Song J, Guan C and Luo X** (2021) Active transmission/absorption frequency selective surface with dynamical modulation of amplitude. *IEEE Transactions on Antennas and Propagation* **69**(6), 3593–3598.
31. **Pereira VM, Hardt LG, Fantineli DG Heckler MV, Armas LE**. (2023) Characterization of dielectric properties of graphene and graphite using the resonant cavity in 5G test band. *Journal of Microwaves, Optoelectronics and Electromagnetic Applications* **22**(1), 63–76.
32. **Bellucci S, Maffucci A, Maksimenko S, Micciulla F, Migliore MD, Paddubskaya A, Pinchera D and Schettino F** (2018) Electrical permittivity and conductivity of a graphene nanoplatelet contact in the microwave range. *Materials* **11**(12), 2519.
33. **Rubrice K, Castel X, Himdi M and Parneix P** (2016) Dielectric characteristics and microwave absorption of graphene composite materials. *Materials* **9**(10), 825.
34. **Garg R and Bahl IJ** (1979) Characteristics of coupled microstriplines. *IEEE Transactions on Microwave Theory & Techniques* **27**(7), 700–705.
35. **Kirschning M and Jansen RH** (1984) Accurate wide-range design equations for parallel coupled microstrip lines. *IEEE Transactiions On* **MTT-32**, 83–90. see also corrections, IEEE Trans., Vol. MTT-33, 1985, p. 288.

Sai Haranadh Akkapanthula is pursuing his Ph.D. in the Department of Electrical Engineering with specialization in RF & Microwave Engineering at Indian Institute of Technology Tirupati, India. He completed his M. Tech in Communication Engineering and Signal Processing at VR Siddhartha Engineering College, Vijayawada, in 2020. His current research areas include designing and developing of tunable microwave components using electric and magnetic materials like ferrites, graphene etc.

Srujana Kagita received her Ph.D. in RF & Microwave domain from IIT Delhi in 2016. She completed her master degree from Arizona State University in 2009. Currently she is an assistant professor in Department of electrical engineering at IIT Tirupati. Her research interests include tunable microwave circuits using materials like ferrites, graphene, etc. and the development of compact tunable Low Temperature Co-fired Ceramic (LTCC) microwave components.